

The Tropical Eastern Pacific Seasonal Cycle: Assessment of Errors and Mechanisms in IPCC AR4 Coupled Ocean–Atmosphere General Circulation Models*

SIMON P. DE SZOEKE

NOAA/Earth System Research Laboratory, Boulder, Colorado

SHANG-PING XIE

International Pacific Research Center, and Department of Meteorology, University of Hawaii at Manoa, Honolulu, Hawaii

(Manuscript received 28 March 2007, in final form 11 September 2007)

ABSTRACT

Warmer SST and more rain in the Northern Hemisphere are observed year-round in the tropical eastern Pacific with southerly wind crossing the equator toward the atmospheric heating. The southerlies are minimal during boreal spring, when two precipitation maxima straddle the equator. Fourteen atmosphere–ocean coupled GCMs from the Coupled Model Intercomparison Project (CMIP3) and one coupled regional model are evaluated against observations with simple metrics that diagnose the seasonal cycle and meridional migration of warm SST and rain. Intermodel correlations of the metrics elucidate common coupled physics. These models variously simulate the climatology of SST and ITCZ rain.

In 8 out of 15 models the ITCZ alternates symmetrically between the hemispheres with the seasons. This seasonally alternating ITCZ error generates two wind speed maxima per year—one northerly and one southerly—resulting in spurious cooling in March and a cool SST error of the equatorial ocean. Most models have too much rain in the Southern Hemisphere so that SST and rain are too symmetric about the equator in the annual mean. Weak meridional wind on the equator near the South American coast (2°S–2°N, 80°–90°W) explains the warm SST error there.

Northeasterly wind jets blow over the Central American isthmus in winter and cool the SST in the eastern Pacific warm pool. In some models the strength of these winds contributes to the early demise of their northern ITCZ relative to observations. The February–April northerly wind bias on the equator is correlated to the antecedent December–February Central American Pacific wind speed at -0.88 . The representation of southern-tropical stratus clouds affects the underlying SST through solar radiation, but its effect on the meridional atmospheric circulation is difficult to discern from the multimodel ensemble, indicating that errors other than the simulation of stratus clouds are also important for accurate simulation of the meridional asymmetry.

This study identifies several features to be improved in atmospheric and coupled GCMs, including the northeasterly cross-Central American wind in winter and meridional wind on the equator. Improved simulation of the seasonal cycle of meridional wind could alleviate biases in equatorial SST and improve simulation of ENSO and its teleconnections.

1. Introduction

Easterly trade winds blow over most of the tropical Pacific Ocean so that through Ekman divergence cold

water upwells on the equator. In dynamic balance with the easterly wind stress on the equator, sea level tilts up to the west and the thermocline shoals in the east, resulting in an SST gradient with cooler SST in the east. Atmospheric convection and wind variability respond to SST gradient variability, and thereby coupled equatorial modes contribute to upper-ocean and SST anomalies and to El Niño–Southern Oscillation (ENSO), the leading mode of interannual climate variability on the globe (Neelin et al. 1998; Wallace et al. 1998).

Errors in the simulation of ENSO are often attributed to errors in the mean state (AchutaRao and Sperber

* International Pacific Research Center/School of Ocean and Earth Science and Technology Publication Number 480/7202.

Corresponding author address: Simon de Szoeke, NOAA/ESRL/PSD3, 325 Broadway, Boulder, CO 80305.
E-mail: simon.deszoeke@noaa.gov

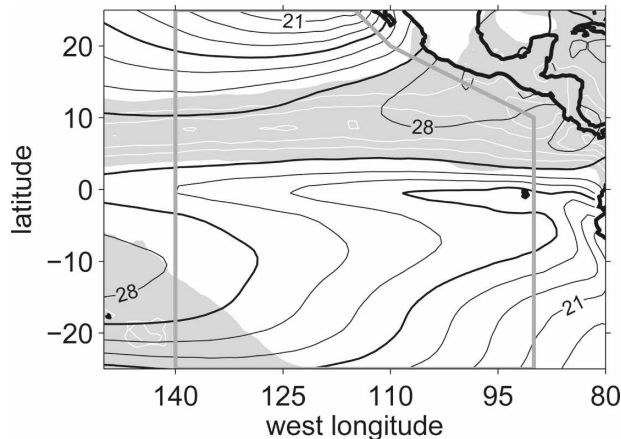


FIG. 1. Annual mean Reynolds SST (interval 1°C ; 24° and 27°C contours are thickened) and TRMM 3B43 merged rain (shaded above 2 mm day^{-1} ; contour interval 2 mm day^{-1}) in the tropical eastern Pacific region. The gray box shows the region used for the zonal averages and meridional asymmetry indices.

2006; Wittenberg et al. 2006; Guilyardi 2006). ENSO has its largest interannual SST anomaly in the tropical eastern Pacific during December, when changes in the heating over the tropical eastern Pacific affect the location of the winter storm track over North America (Horel and Wallace 1981; Wallace and Gutzler 1981). Many coupled general circulation models (CGCMs) simulate ENSO variability in the wrong season (Saji et al. 2006) so that ENSO cannot affect the Northern Hemisphere storm track as observed. Accurate simulation of the behavior and seasonality of ENSO and its teleconnections then requires accurate simulation of the tropical Pacific mean state and seasonal cycle.

The tropical eastern Pacific climate is highly asymmetric about the equator with warmer SST and more precipitation observed in the Northern Hemisphere. Figure 1 shows the annual-average distribution of SST and rain. The northwest–southeast slant of the American coast breaks the meridional symmetry of the eastern Pacific climate (Philander et al. 1996; Okajima et al. 2003). Alongshore southeasterly trade winds drive offshore Ekman transport and cold water upwelling along the coast in the Southern Hemisphere, and coupled ocean–atmosphere feedbacks amplify the asymmetry and spread it westward (Xie and Saito 2001). Blocked by the Andes, the zonal trade winds are weak near the South American shore and the equatorial ocean there is partly cooled by upwelling south of the equator, driven by southerly wind stress (Philander and Pacanowski 1981). The meridional asymmetry keeps the cross-equatorial wind southerly year round, a key condition for the generation of an annual cycle in SST on the equator (Mitchell and Wallace 1992; reviewed by Xie 2004).

Mechoso et al. (1995) compared the simulations of 11 CGCMs in the eastern Pacific and found that, rather than reproducing the observed seasonal cycle of SST and precipitation, models were susceptible to a “double ITCZ” error, with persistent zonal bands of precipitation in each hemisphere. The observed meridional asymmetry, with warmer SST and more precipitation in the north, was typically not simulated. Much progress has been made during the past decade in CGCM development. In particular, most of the current-generation CGCMs include global ocean GCMs without flux adjustment.

The present study evaluates the simulation of the eastern tropical Pacific and its seasonal cycle by a systematic analysis of state-of-the-art CGCMs from the World Climate Research Programme (WCRP) third Coupled Model Intercomparison Project (CMIP3). This study provides metrics of model agreement with observations for the seasonal and meridional distribution of rain and SST in the tropical eastern Pacific.

In addition to the double ITCZ, a cold SST error on the equator and extension of the cold tongue too far west relative to observations has been identified and associated with a double-ITCZ error in the western Pacific (Mechoso et al. 1995; Davey et al. 2002; Wittenberg et al. 2006; Dai 2006). In an analysis of feedbacks, Lin (2007) attributes these errors to overly strong wind speed and sensitivity of rain to SST and too-weak damping of SST by evaporation and solar shading by clouds. Other errors have been identified, such as a warm SST error in the coastal upwelling region offshore of Peru (Gordon et al. 2000b; Large and Danabasoglu 2006), often compounded by a deficit of stratocumulus clouds (Ma et al. 1996; Gordon et al. 2000b) and by errors in the alongshore wind. Errors in the wind could occur for a variety of reasons, including poor resolution of the Andes (Xu et al. 2004; Richter and Mechoso 2006). Errors in the meridional and seasonal distribution of atmospheric heating are communicated to equatorial SST by the meridional cross-equatorial wind. This study computes indices of these errors from the result of each model and examines interactions among errors.

We take a recent approach to model comparison that considers each of the models as a realization from an ensemble of physical representations of the eastern Pacific. Differences among model physics and configuration perturb their solutions, and some perturbations are systematically amplified by feedbacks that exist in both modeled and observed climate systems. The spread of simulated solutions can thus be used to diagnose physical mechanisms responsible for the climate. This type of analysis complements deterministic numerical model

TABLE 1. A list of the 15 models compared in this study.

Modeling center	Model abbreviation	Reference
Canadian Centre for Climate Modelling and Analysis	CCCMA CGCM3.1	(Flato and Boer 2001)
Centre National de Recherches Météorologiques (France)	CNRM-CM3	(Salas-Méla et al. 2005)
CSIRO Atmospheric Research (Australia)	CSIRO Mk3.0	(Cai et al. 2005)
Geophysical Fluid Dynamics Laboratory (United States)	GFDL CM2.0	(Delworth et al. 2006)
Geophysical Fluid Dynamics Laboratory	GFDL CM2.1	(Delworth et al. 2006)
Met Office Hadley Centre for Climate Prediction and Research (United Kingdom)	UKMO HadCM3	(Gordon et al. 2000a)
Institute of Atmospheric Physics (China)	IAP FGOALS 1.0g	(Yu et al. 2004)
Institute of Numerical Mathematics (Russia)	INM-CM3.0	(Diansky and Volodin 2002)
L'Institut Pierre-Simon Laplace (France)	IPSL CM4	(Goosse and Fichet 1999)
Center for Climate System Research (Japan)	MIROC3.2(medres)	(Nozawa et al. 2005)
Center for Climate System Research	MIROC3.2(hires)	(Nozawa et al. 2005)
Meteorological Research Institute (Japan)	MRI CGCM2.3.2	(Yukimoto et al. 2001)
National Center for Atmospheric Research (United States)	NCAR CCSM3.0	(Collins et al. 2006)
National Center for Atmospheric Research	NCAR PCM1	(Meehl et al. 2005)
International Pacific Research Center (United States/Japan)	IROAM	(Xie et al. 2007)

experiments in which physical conditions or parameterizations are changed to diagnose cause and effect in the climate system.

The remainder of this paper is organized as follows. In section 2 simulations of current state-of-the-art coupled models are presented and compared for the tropical eastern Pacific region. Metrics are introduced for the seasonal and meridional distribution of SST and rain in the tropical eastern Pacific. In section 3 model errors in the meridional wind and equatorial SST are assessed, and mechanisms linking equatorial errors to the meridional distribution of heating are described. Northern Hemisphere SST cooling from strong Central American gap winds and Southern Hemisphere warming due to too little stratus cloud are assessed as contributors to the lack of meridional asymmetry in models. Section 4 summarizes the conclusions.

2. Comparison and assessment of coupled models in the tropical eastern Pacific

a. Models and data

In this study we compare SST, rain, and wind for the 15 coupled models listed in Table 1. With the exception of the International Pacific Research Center (IPRC) Regional Ocean–Atmosphere Model (IROAM) of the tropical eastern Pacific (Xie et al. 2007), all of the models are global atmosphere–ocean CGCMs whose twentieth-century Climate in Coupled Models scenario (20C3M; additional information is available online at http://www-pcmdi.llnl.gov/projects/cmip/ann_20c3m.php) simulation has been submitted to CMIP3. CMIP3 CGCM simulations were submitted to the Program for Climate Model Diagnosis and Intercomparison

(PCMDI) for inclusion in the Intergovernmental Panel on Climate Change Fourth Assessment Report (IPCC AR4), and can be downloaded from links to the PCMDI Web site (<http://www-pcmdi.llnl.gov/>). The 20C3M simulations are spun up and then forced by solar, volcanic, direct sulfate aerosol, and greenhouse gas forcings for the calendar years 1900–99. The climatologies presented are monthly averages over this 100-yr period. The Meteorological Research Institute CGCM version 2.3.2 (MRI CGCM2.3.2; Yukimoto et al. 2001) performs flux adjustment for heat, water, and momentum; the Canadian Centre for Climate Modeling and Analysis CGCM version 3.1 (CCCMA CGCM3.1; Flato and Boer 2001) performs heat and water flux adjustment; and the Institute of Numerical Mathematics Coupled Model version 3.0 (INM-CM3.0; Diansky and Volodin 2002) performs flux adjustment for water. All other GCMs are coupled freely without flux correction.

IROAM consists of a tropical Pacific Ocean basin model (Modular Ocean Model version 2; Pacanowski 1995; Pacanowski and Griffies 2000) and a regional atmospheric model (RAM; Wang et al. 2003, 2004a) forced by the National Centers for Environmental Prediction–National Center for Atmospheric Research (NCEP–NCAR) reanalysis (Kistler et al. 2001) at its lateral boundaries (35°N/S, 150°–30°W). Fluxes over the western half of the Pacific Ocean are derived from NCEP reanalysis. The surface salinity is relaxed toward climatology (Levitus and Oort 1977). The IROAM is initialized in 1996, and climatologies are averaged over the six years 1998–2003, which excludes the strong ENSO event in late 1997.

Simulations were compared with observations of SST, surface precipitation (rain), and surface wind. The

SST data are the NOAA Optimal Interpolation SST (OISST), interpolated from 2° in situ data from 1971–2000 and 1° satellite data from 1982–2000 (Reynolds et al. 2002; additional information is available online at <http://www.cdc.noaa.gov/cdc/data.noaa.oisst.v2.html>). The rain climatology is from the NASA Tropical Rainfall Measuring Mission (TRMM) 3B43 product, which combines observations from the TRMM satellite instruments with Global Precipitation Climatology Center (GPCC) rain gauge observations to make 1° monthly estimates of precipitation for 1998–2003 (Adler et al. 2000; additional information is available online at http://disc.sci.gsfc.nasa.gov/precipitation/TRMM_README/). The wind observations are the climatology from August 1999 through August 2006 of 1° monthly Quick Scatterometer (QuikSCAT) Ku-band satellite scatterometer retrievals (additional information is available online at <http://www.remss.com>).

b. Seasonal–meridional ITCZ pattern comparison

Previous studies have shown model results with a double ITCZ in the annual mean, rather than the single observed northern ITCZ (Fig. 1). Because of the zonal symmetry of the climate in the eastern Pacific, we zonally average within the box shown in Fig. 1 (25°S – 25°N , 140° – 90°W , with the northeast vertex cut off to exclude continental effects of Central America). Figure 2 shows the zonally and annually averaged SST and rain in the tropical eastern Pacific for each of the models (black lines) and the observations (gray). While the model SST was distributed symmetrically within 2°C of observations, the rain in the models tends to be ~ 2 mm day^{-1} higher than the satellite estimate in the Northern Hemisphere. The observed ITCZ at 5°S is less than 2 mm day^{-1} in the annual average; yet most models make this southern ITCZ stronger and farther south—typically 3–5 mm day^{-1} in the neighborhood of 10°S .

The seasonal cycle is obscured by the annual average in Figs. 1 and 2. As expected from the meridional migration of the sun, the meridional distribution of SST and rain vary with season. Figure 3 (0) shows contours of the observed SST and rain distribution with latitude for each month. Year round in the Northern Hemisphere, the SST is 27° – 29°C and the rainfall exceeds 4 mm day^{-1} . In the Southern Hemisphere the SST is always less than 28°C . Briefly in March and April there is an *observed* double ITCZ when the northern ITCZ is weakest and rain is nearly symmetric about the equator and exceeds 4 mm day^{-1} in both hemispheres.

Each of the other panels in Fig. 3 depicts the seasonal–meridional distribution of SST and rain for one of the models listed in Table 1. There is qualitative improvement in these simulations compared to those ana-

lyzed by (Mechoso et al. 1995), but the simulations still represent the seasonal cycle of SST and precipitation in a variety of ways. We divide the model simulations into three main categories based in their seasonal cycle of precipitation: a *persistent double ITCZ* error in which rain persists too long in the Southern Hemisphere, an *alternating ITCZ* error, and qualitative agreement with observations.

Three models, from Centre National de Recherches Météorologiques (CNRM), the Institute of Atmospheric Physics (IAP), and INM exhibit a bias toward a persistent double ITCZ, like many of the simulations studied in 1995. Persistent double ITCZ simulations are those in which rain in the Northern Hemisphere continuously exceeds 4 mm day^{-1} and rain in the Southern Hemisphere persists too long, exceeding 4 mm day^{-1} for at least 4 months.

Eight of the 15 simulations produce an alternating ITCZ with SST and precipitation maxima that cross the equator with the seasons. These simulations have a northern ITCZ in boreal fall (roughly July–November) that breaks up and forms a southern ITCZ in boreal spring (February–May). Alternating ITCZ simulations are defined as those whose minimum monthly precipitation in the Northern Hemisphere is less than 4 mm day^{-1} . The CCCMA, Commonwealth Scientific and Industrial Research Organisation model Mark version 3.0 (CSIRO Mk3.0), L’Institut Pierre-Simon Laplace Coupled Model version 4 (IPSL CM4), Model for Interdisciplinary Research on Climate 3.2, medium-resolution version [MIROC3.2(medres)], both Geophysical Fluid Dynamics Laboratory (GFDL) Climate Models [versions 2.0 (CM2.0) and 2.1 (CM2.1)], and both NCAR models [Community Climate System Model version 3 (CCSM3) and Parallel Climate Model version 1 (PCM1)] all show this most common error. These simulations exhibit different amounts of meridional asymmetry. Some, like the CCCMA model [Fig. 3 (1)], have a stronger northern ITCZ; others, like the PCM1 (Fig. 3d), have nearly symmetric ITCZs that alternate between the hemispheres. In the annual average, the alternating ITCZ error looks like the persistent double ITCZ error, with the southern ITCZ in boreal spring contributing the annual-average southern ITCZ. The different effects on the wind and on the ocean of an alternating ITCZ opposed to a persistent double ITCZ are explored in section 3.

Two models, the Met Office (UKMO) Third Hadley Centre Coupled Ocean–Atmosphere GCM (HadCM3) and the IROAM, qualitatively reproduce the observed dominance of the northern ITCZ and the brief March–April double ITCZ. Both have realistic seasonal cycles of SST. The UKMO SST is qualitatively correct, but

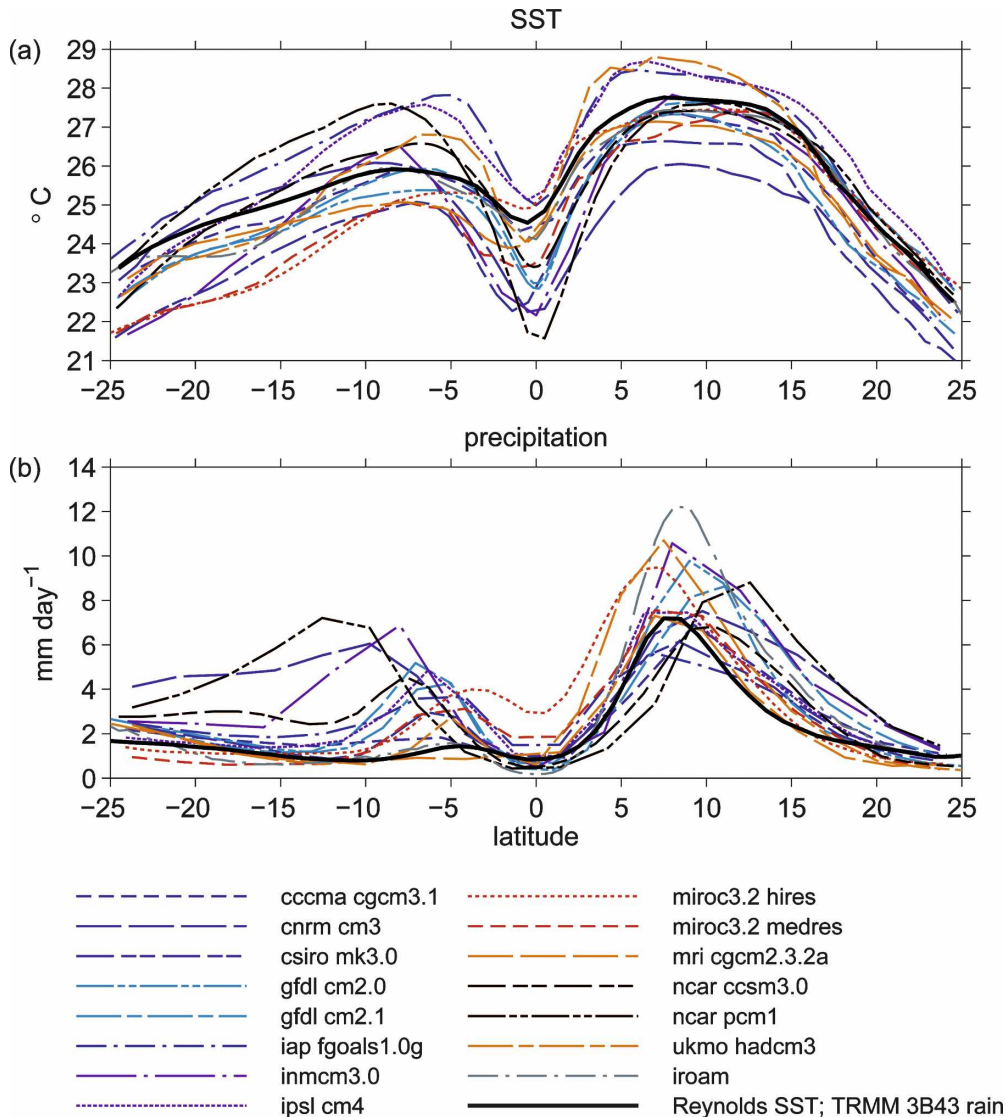


FIG. 2. Seasonally and zonally averaged (a) SST and (b) precipitation in the eastern Pacific (140°–90°W region indicated in Fig. 1) for 15 models (broken colored lines) and observations (solid black line).

almost 1°C too warm. Its southern ITCZ persists into May. The IROAM has an overactive hydrological cycle, with precipitation roughly double the TRMM 3B43 merged precipitation retrieval. (Though the spatial pattern of precipitation over the eastern Pacific has not changed significantly in recent estimates, the magnitude of the TRMM 3B43 retrieval has been scaled back considerably relative to previous TRMM satellite estimates. Models might be poorly tuned to give precipitation magnitudes in agreement with TRMM 3B43, so we focus our analysis on the spatial and temporal pattern of simulated rain.)

Two remaining models do not fit neatly into the three categories. The MIROC3.2 high-resolution ver-

sion (hires) ITCZ migrates meridionally like an alternating ITCZ but, like a persistent double ITCZ, it lasts longer than four months in the Southern Hemisphere and is continuous in the Northern Hemisphere. The MIROC3.2(hires) has more than 6 mm day⁻¹ of rain on the equator in April and May. No other model examined here has equatorial rain reaching 4 mm day⁻¹. The MRI model has precipitation in the Northern Hemisphere similar to observations, but never has intense precipitation in the Southern Hemisphere.

c. Metrics for the seasonal cycle

The model errors in Fig. 3 can be summarized by the correlation of the spatial–seasonal distribution of rain

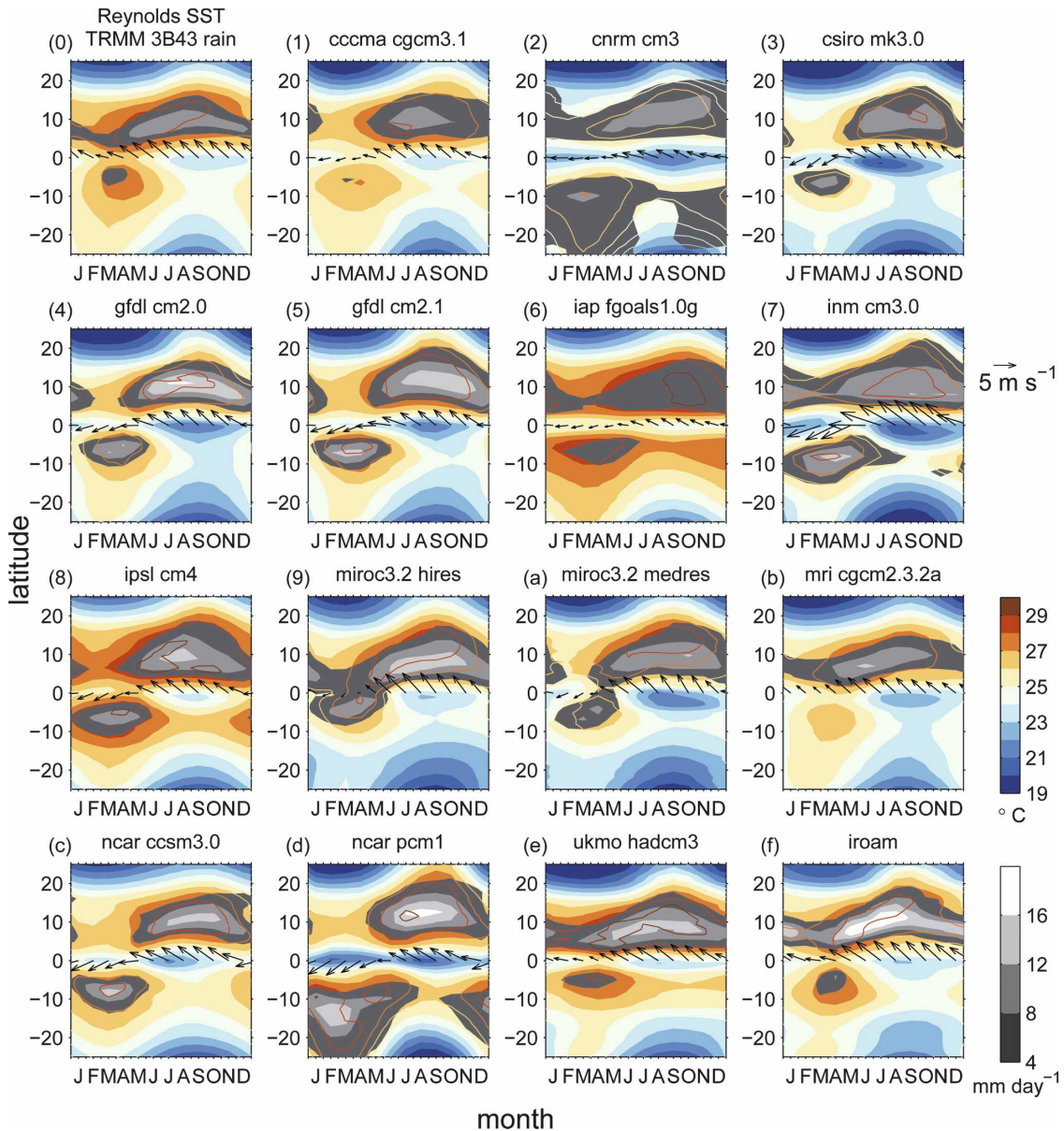


FIG. 3. Seasonal cycle of the meridional distribution of SST (color contours and shading; interval of 1°C) and rain (gray shaded above 4 mm day^{-1} ; interval of 4 mm day^{-1}) over the tropical eastern Pacific ($140^{\circ}\text{--}90^{\circ}\text{W}$ region in Fig. 1). Equatorial wind vectors are shown for each month. (0) Observations; (1)–(f) seasonal cycle in the model simulations as listed in Table 2.

to the observations in a Taylor (2001) diagram (Fig. 4). Observations were spatially collocated to the latitude grid of each model, and the standard deviation of the meridional–seasonal pattern and the correlation of the model pattern with observations were computed. Interpolating all model results to the grid of observations (not shown) negligibly affected the statistics. The statistics for rain (gray) are computed over $\pm 25^{\circ}$ latitude. Errors in SST are confined closer to the equator than rain errors, so the pattern correlation of the SST (black)

is computed over $\pm 10^{\circ}$ latitude. The distance from the point at unity on the abscissa (marked with a circle) is the normalized rms error (NRMSE) of each model relative to observation. The NRMSE for SST and rain are shown in Table 2.

The NRMSE of SST in the models is typically smaller than that of rain. The seasonal–meridional pattern of SST of most models is correlated to observations around 0.9. We expect rain to be more challenging for models because it depends not only on the pattern of

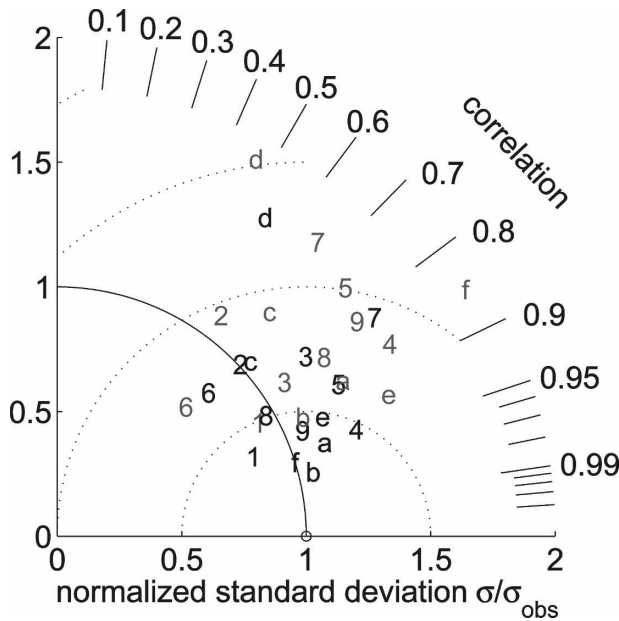


FIG. 4. Taylor diagram of normalized rms amplitude and correlation of the model seasonal–meridional pattern (Fig. 3) to observations of SST ($\pm 10^\circ\text{N}$, black) and precipitation ($\pm 25^\circ\text{N}$, gray) for the eastern tropical Pacific region $140^\circ\text{--}90^\circ\text{W}$. A model in perfect agreement with observations would lie on the abscissa at amplitude 1 (marked with circle); the distance from this point is the model NRMSE (dotted lines). Symbols for models and observations are listed in Table 2.

SST, but also on atmospheric dynamics and parameterizations of atmospheric convection. Correlations of rain to observations are typically around 0.8. Some of the error in the rain pattern is due to model error in the absolute magnitude of precipitation, even though the spatial and temporal distribution of rain is well correlated to observation. All models overestimate the magnitude of mean rain in the region, some [CNRM-version 3 (CM3), INM-CM, PCM1, and IROAM] by a factor of 2. Normalizing the mean rain of the models to observation reduces their standard deviation without changing their correlation to observations, reducing the error of most models. Upcoming versions of atmospheric models will likely be better tuned to reflect recent observational estimates of rain over the oceans.

Metrics shown in the Taylor diagram (Fig. 4) economically summarize errors in the meridional–seasonal pattern of rain and SST in the tropical eastern Pacific. Further diagnostics show the character of the errors. There is considerable variety in the meridional asymmetry of rain and SST simulated by the models in Fig. 3. The fidelity of the simulations in the tropical eastern Pacific is diagnosed by the annual-mean meridional asymmetry index and the seasonal cycle of the asymmetry index. The meridional rain asymmetry index

TABLE 2. Legend of symbols used for models and observations in scatterplots, and the NRMSE of each model's seasonal–meridional pattern of SST and rain, respectively to Reynolds SST and TRMM 3B43 rain. The category of the seasonal–meridional rain pattern is shown in the rightmost column.

Symbol	Model	NRMSE		Category
		SST	Rain	
1	CCCMA CGCM3.1	0.38	0.49	A
2	CNRM-CM3	0.74	0.95	P
3	CSIRO MK3.0	0.72	0.62	A
4	GFDL CM2.0	0.47	0.84	A
5	GFDL CM2.1	0.62	1.01	A
6	IAP FGOALS1.0G	0.70	0.71	P
7	INM-CM3.0	0.92	1.18	P
8	IPSL CM4	0.51	0.72	A
9	MIROC3.2(hires)	0.42	0.88	
a	MIROC3.2(medres)	0.38	0.64	A
b	MRI CGCM2.3.2A	0.26	0.48	
c	NCAR CCSM3.0	0.74	0.91	A
d	NCAR PCM1	1.29	1.53	A
e	UKMO HadCM3	0.48	0.66	O
f	IROAM	0.30	1.10	O
0	Observed			

(north–south) is defined for each month as the average rain from the equator to 25°N minus the rain from the equator to 25°S , likewise for SST. Figure 5 shows the seasonal cycle of the asymmetry index of rain and SST for models ranked from lowest to highest NRMSE of SST (Table 2). The meridional wind on the equator is shown in the lower middle axis of Fig. 5. The error category of the models determined from Fig. 3 is shown above the SST asymmetry index: *A* for alternating ITCZ, *P* for persistent double ITCZ, and *O* for near observations. Models with rain patterns resembling observations have NRMSE below the median, while those categorized as having persistent double ITCZs have NRMSE above the median.

Observations of the meridional asymmetry indices and equatorial wind indices are shown by the gray shaded areas. The midline of the gray shading is the observed annual mean. The observed SST asymmetry lags the solar seasonal cycle by 2–3 months, with most northward asymmetry (positive index) in September and least northward asymmetry in March, when the SST and rain indices are nearly zero (symmetric) and rain falls equally on each side of the equator. The northernmost asymmetry of rain in August leads the asymmetry of SST by one month, perhaps due to the remote influence of heating of the North American continent, which warms faster than the ocean.

Models with higher NRMSE of SST (positioned to the right in Fig. 5) tend to have too little mean meridional asymmetry, approaching equal SST and rain in

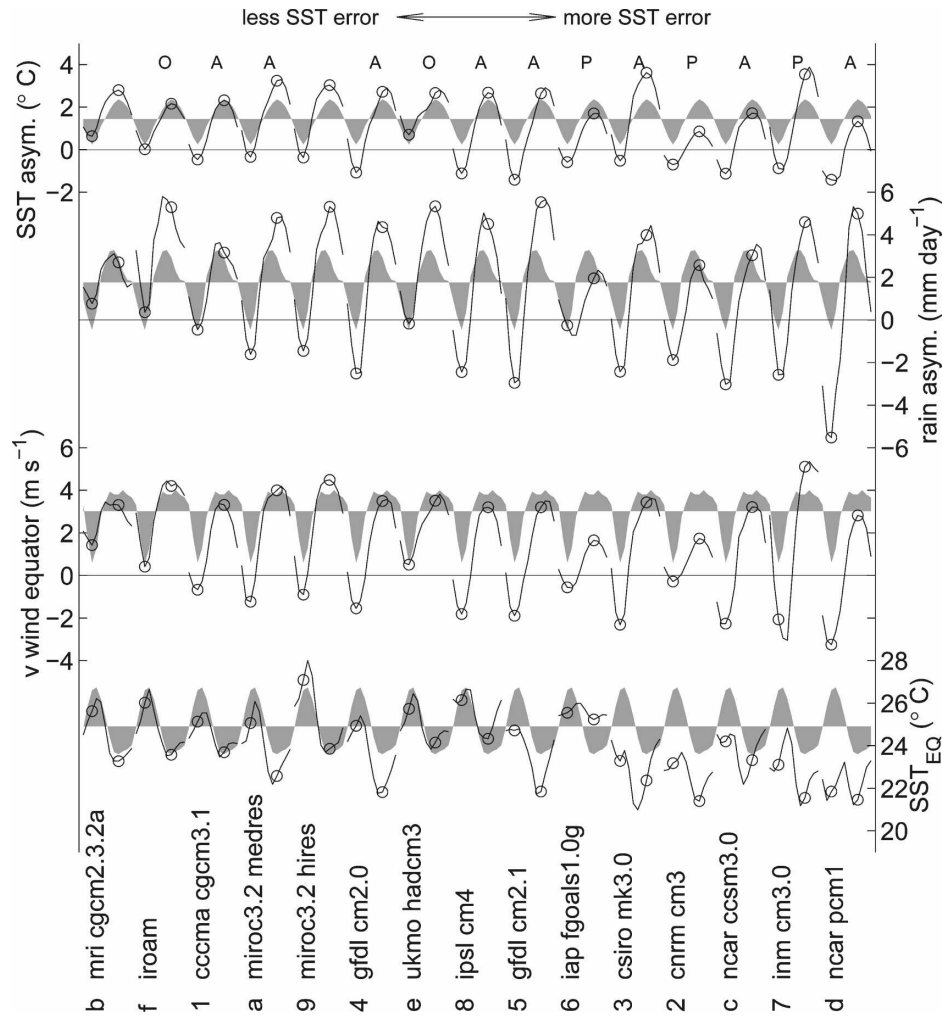


FIG. 5. The seasonal progression of the tropical eastern Pacific meridional asymmetry (from 25°N–equator to 25°S–equator, 140°–90°W region shown in Fig. 1) of rain (mm day⁻¹, top) and SST (°C, second axis from top) for each of the models. Models are ranked from left to right by lowest to highest NRMSE of the seasonal–meridional SST pattern. The seasonal cycle of meridional wind (m s⁻¹) and SST on the equator ($\pm 2^\circ$ lat) are on the lower two axes. March and September, the months of observed extreme SST asymmetry index, are circled.

the north and south over the year, and too large a meridional seasonal cycle. The March–August asymmetry index difference explains about 80% of the rms error of the seasonal cycle of both SST and rainfall asymmetry. The seasonal cycle of asymmetry is responsible for more error than the annual-average double ITCZ in the eastern Pacific. The meridional wind points toward warm SST and the ITCZ, so it is an indicator of the meridional asymmetry. The equatorial wind vectors in Fig. 3 show that most of the annual cycle of wind is in the meridional component. Figure 6 shows the high correlation of the annual-mean equatorial meridional wind with the annual mean asymmetry of SST and rain among the models ($r = 0.78$ and 0.83 , respectively). The

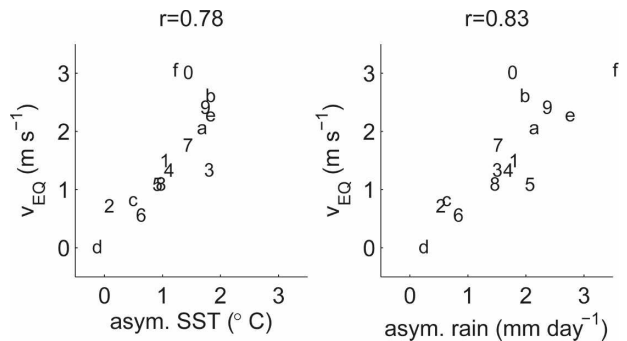


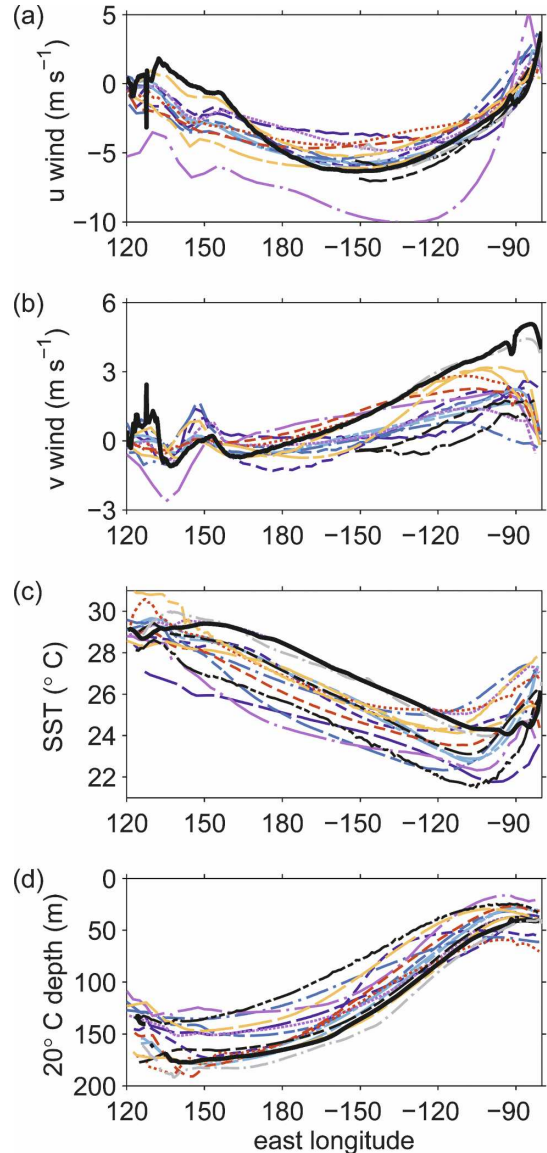
FIG. 6. Annual mean meridional asymmetry of SST and rain (140°–90°W) in Fig. 2 vs equatorial ($\pm 2^\circ$ lat) meridional wind.

annual mean meridional asymmetry of SST and precipitation are correlated at 0.77 (not shown). In March, only the MRI, IROAM, and UKMO models maintain southerly cross-equatorial wind and positive SST asymmetry as observed. All other models show northerly wind and negative meridional asymmetry in March. Though the heating asymmetry predicts the meridional wind well, the observed wind in Fig. 6 lies significantly above the regression line predicted by the asymmetry. We speculate that models simulate weak equatorial wind for a variety of reasons, including misrepresentation of ageostrophic flow trapped against the Andes, too-strong surface stress related to inadequate vertical resolution, and inadequate resolution of local circulations, such as that due to the sharp SST front north of the equator (de Szoeke and Bretherton 2004; Small et al. 2005).

The southerly cross-equatorial wind observed by QuikSCAT has a long season of 3–4 m s⁻¹ southerlies and a brief season of southerlies less than 1 m s⁻¹. Strong southerly wind lasts from July to November, when winds converge on warm SST in the northeastern tropical Pacific. The range of wind estimates among QuikSCAT, Tropical Atmosphere Ocean (TAO) buoys, and NCEP–NCAR and NCEP–Department of Energy (DOE) reanalyses is on the order of 1 m s⁻¹, and the 6-yr (1999–2006) climatology estimated from QuikSCAT seems to be representative of longer averages based on dividing longer reanalysis time series (not shown). QuikSCAT meridional wind is systematically about 1 m s⁻¹ stronger than winds measured by the TAO buoys. The higher QuikSCAT wind could reflect stronger mean wind stress due to variable ocean currents (Polito et al. 2001) and SST.

3. Equatorial errors: Effect of asymmetry on the equatorial wind and ocean

Mean easterly trade winds deepen the ocean thermocline in the western Pacific equator and shoal the thermocline in the east. Figure 7a shows the zonal trade winds on the equator over the Pacific Ocean ($\pm 2^\circ$ latitude), which are easterly (negative) over most of the Pacific, resulting in the tilt of the 20°C isotherm (Fig. 7d) and warmer SST toward the west (Fig. 7c). The black lines in Fig. 7d are the 20°C isotherm depth from the Simple Ocean Data Assimilation (SODA) (Carton et al. 2000a,b). Most models represent the zonal structure of equatorial easterlies well compared to observations but represent the equatorial SST with less fidelity. Almost all models have a 20°C isotherm that is 50 m too shallow in the western and central Pacific and tens of meters too shallow in the eastern Pacific. The shallow



- cccma cgcm3.1
- cnrm cm3
- csiro mk3.0
- gfdl cm2.0
- gfdl cm2.1
- iap fgoals1.0g
- inm cm3.0
- ipsl cm4
- miroc3.2 hires
- miroc3.2 medres
- mri cgcm2.3.2a
- ncar ccs3.0
- ncar pcm1
- ukmo hadcm3
- iroam
- Observation

FIG. 7. Zonal sections of (a) zonal wind, (b) meridional wind, (c) SST, and (d) 20°C isotherm depth for the Pacific Ocean along the equator ($\pm 2^\circ$). Each model result is indicated by a broken colored line. Observations are shown by the solid black line. Wind observations are from QuikSCAT, SST from Reynolds, and 20°C isotherm depth from SODA.

thermocline is associated with cold SST errors of 1° – 3°C in the central Pacific. Models also overestimate the eastward warming in the eastern Pacific. The stronger than observed eastward warming compensates the central Pacific cold error and results in a 1° – 2°C warm SST error in most models. These errors in the annual average are discussed by Mechoso et al. (1995), Davey et al. (2002), and AchutaRao and Sperber (2006). The sensitivity of SST to ENSO modes depends on the depth of the thermocline, the stratification, and the strength of upwelling and mixing (Meehl et al. 2001).

Because the thermocline shoals in the east, SST there is sensitive to the vertical ocean circulation. Easterly winds drive divergent poleward Ekman transport on either side of the equator, resulting in equatorial upwelling that is partly responsible for the tongue of cold water on the equator. Cross-equatorial meridional wind is also responsible for cooling the ocean in three ways. First, higher scalar wind speed increases evaporation from the ocean surface. Second, stronger scalar wind stress drives turbulent vertical mixing, which entrains cold water into the surface mixed layer, especially where the thermocline is shallow and has strong temperature stratification. We examine a third mechanism, by which meridional wind stress drives a meridional-vertical circulation in the ocean (Philander and Pacanowski 1981; Philander and Delecluse 1983). Southerly winds cause zonal Ekman transport either side of the equator but push surface water northward directly on the equator. This results in a meridional divergence and upwelling on the windward south side of the equator and convergence and downwelling on the north side. The net result of this wind-driven meridional circulation is to cool the surface temperature on and slightly upwind of the equator. The influence of the meridional cell on the meridional tilt of the thermocline is estimated by the difference (asymmetry) of the 20°C isotherm depth from the equator to 3°N minus that from the equator to 3°S , from 80° – 90°W . The intermodel correlation of meridional wind to thermocline asymmetry is greater than 0.69 in all seasons. In addition, $\pm 3^{\circ}$ latitude SST is significantly predicted by the 20°C isotherm asymmetry.

As the meridional wind varies with season, so does the meridional cell in the ocean. The seasonal cycle of meridional wind and thermocline asymmetry, from 80° – 90°W within 3° latitude of the equator, demonstrates the effect of the meridional cell (Fig. 8). In observations and all models except CNRM, seasonal variations in the meridional wind predict the thermocline asymmetry (gray lines), with correlations of at least 0.87. The meridional cell cools SST, so strong negative correlations are observed between ther-

mocline asymmetry and SST (black lines). The median correlation of thermocline asymmetry with SST over the seasonal cycle is -0.83 . For most of the models with weak correlations, negative meridional wind drives the meridional cell backward early in the year with upwelling in the north and thermocline deepening in the south. Since this inverted thermocline asymmetry is also associated with upwelling and advection of cool water onto the equator, these models have a physically consistent lobe of anomalously cool SST in the spring.

a. Seasonal cycle errors

The seasonal cycle of surface wind vectors on the equator averaged from 140° – 90°W is shown for observations and for each of the models in the panels of Fig. 3. Figure 5 shows the seasonal cycle of the meridional component of the wind. In observations, the cross-equatorial wind remains southerly year round, and annual variations of its speed excite the annual cycle of SST on the equator by modulating the strength of southerly induced upwelling, wind stirring, and surface evaporation (Xie 1994). The southerly wind is stronger in boreal summer owing to winds converging onto the ITCZ in the Northern Hemisphere. This southerly wind maximum causes the seasonal minimum cold tongue temperature in September [Fig. 3 (0)]. A wind speed minimum is observed in March, followed by a SST maximum in March–April.

While models agree with observations of the equatorial temperature minimum when the ITCZ is farthest north in September, there is more error and divergence among models in March: 12 of the 15 models have northerly winds associated with the spuriously dominant southern ITCZ in boreal spring (Fig. 5). Model c (Fig. 3c) provides an example of the semiannual equatorial ocean response to the reversing meridional wind associated with the alternating ITCZ. Most of the 20C3M simulations have a reduction of the SST in the March–May warm season; four models have two distinct equatorial cold seasons (Fig. 5). The cold error in boreal spring and the semiannual cycle of equatorial SST are associated with the alternating direction of the meridional wind and the alternating ITCZ error. Though weak southerly winds are observed in the climatology, stronger northerly winds in models drive meridional overturning with upwelling north of the equator and southward advection of cold water onto the equator. Meridional wind speed maxima in both September and March each generate meridional overturning in the equatorial ocean and cool the ocean surface. The equatorial ocean thus rectifies the cooling by the alternating meridional wind and develops a net cold

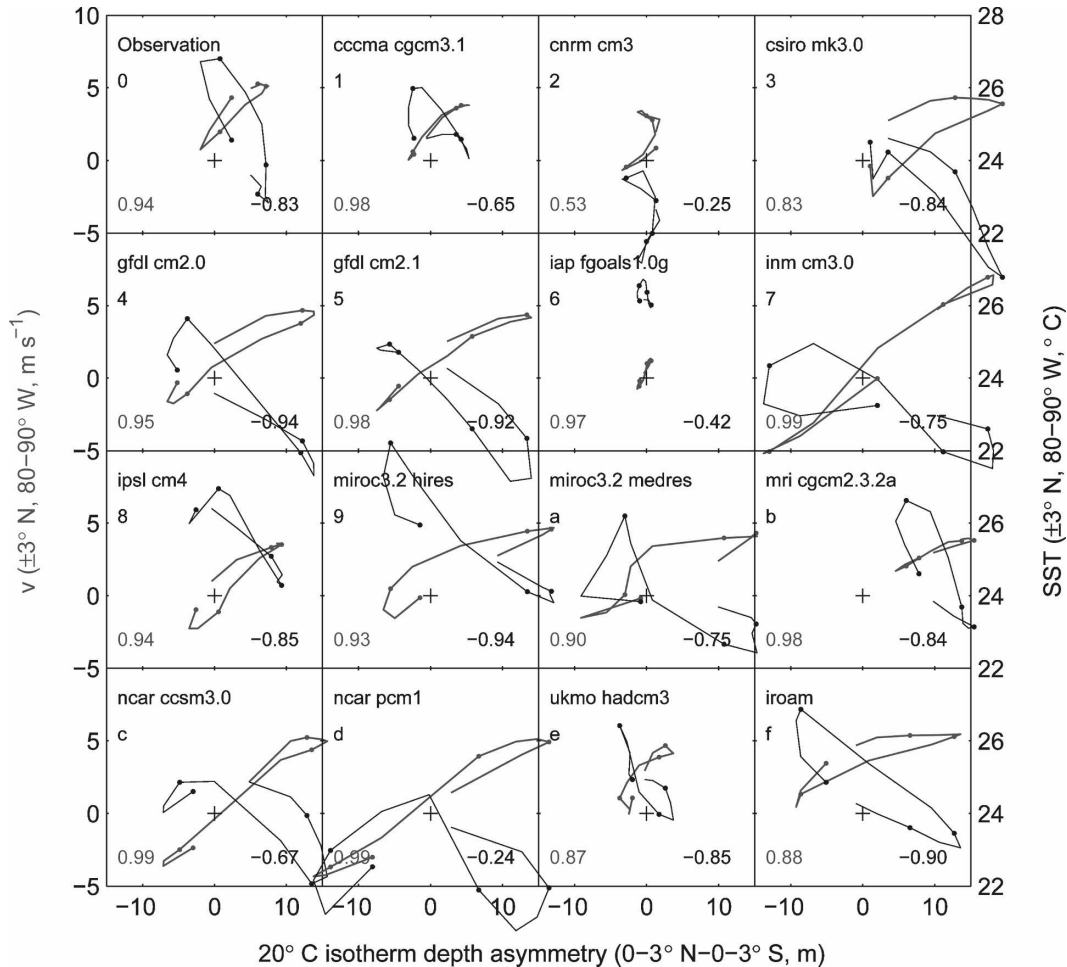


FIG. 8. Seasonal phase diagram of thermocline depth asymmetry (defined as the north – south difference of the average 20°C isotherm depth between 0°–3°N and 0°–3°S, 80°–90°W) on the lower axis; $\pm 3^\circ\text{N}$, 80°–90°W meridional wind (gray; left axis); and $\pm 3^\circ\text{N}$, 80°–90°W SST (black; right axis). The correlation between the thermocline asymmetry and the meridional wind for each model is shown in gray at the lower left of each panel; the correlation of the thermocline asymmetry and the SST is shown at the lower right. January, April, July, and October are marked with dots, and segments connect other months except December–January. The origin of meridional wind and isotherm depth asymmetry is marked with a cross (+).

SST error on the equator (Fig. 7c). The lower two axes of Fig. 5 show that, as models diverge from observations, they tend to have two meridional wind speed maxima and colder mean equatorial SST. Models with the highest rms SST error have two cold seasons.

Among all the models analyzed, cold March SST on the equator ($\pm 2^\circ$ latitude) is correlated to the March wind speed with a coefficient of 0.6 (Fig. 9). (Assuming 15 degrees of freedom for a 95% two-tailed confidence interval, correlations stronger than 0.51 are statistically significant.) March SST varies widely among models from 22° to 27°C, with an intermodel spread in meridional wind speed from 0.5 to 3 m s⁻¹. Intermodel variation is small and statistically insignificant in August and September, so the variation of wind speed among mod-

els in March (Fig. 9) explains their March–August cycle of SST.

b. Meridional wind and equatorial SST east of the Galápagos

Much attention has been paid to the role of coastal upwelling in cooling the ocean at the coast of South America. The results of this section suggest that southerly induced equatorial upwelling is important for cooling the equator between the Galápagos and the South American shore. Figure 10 shows the SST in plan view for observations and model 5 (Table 2). Examples such as model 5 are chosen because they clearly demonstrate the relevant error without being outliers among the models. Though the mean temperature of the cold

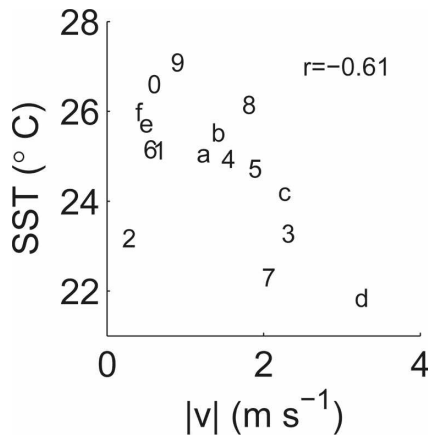


FIG. 9. March eastern Pacific equatorial ($\pm 2^{\circ}\text{N}$, $140^{\circ}\text{--}90^{\circ}\text{W}$) SST ($^{\circ}\text{C}$) vs meridional wind speed (m s^{-1}). Symbols for models and observations are listed in Table 2.

tongue over the eastern Pacific is reasonable, the temperature minimum is displaced westward by some 25° longitude, with a warm error between the Galápagos and the South American shore. This error is common to many state-of-the-art CGCMs (Fig. 7). Kessler et al. (1998) found that blocking ocean advection along the South American coast with a zonal wall along 4.5°S from the coast to 89°W made little difference to the cold tongue, suggesting that the near-shore cold tongue is caused locally by coastal and equatorial upwelling. In another coupled model experiment, Xie (1998) found considerably diminished equatorial upwelling when weakening the meridional wind stress near the coast. In the previous section we showed how the alternating meridional wind can overcool the equator. In this section we diagnose from the model ensemble that southerly wind-driven upwelling is important for cooling equatorial SST east of the Galápagos.

The easterly wind diminishes east of 110°W accord-

ing to QuikSCAT observations (Fig. 10a), even becoming weakly westerly at 80°W . Around 85°W the zonal wind vanishes and the 20°C isotherm levels off at a depth of about 40 m. In this eastern region where the zonal wind stress is small or westerly, the zonal wind stress drives weak surface convergence and downwelling on the equator. Mean meridional wind of 4 m s^{-1} is likely to contribute to upwelling that cools the equator. The zonal wind is well simulated by model 5 (Fig. 10b), but there are errors in the meridional wind. The mean meridional wind in QuikSCAT is about 5 m s^{-1} east of 90°W , but it is less than 1.5 m s^{-1} in model 5. According to Fig. 7b, all GCMs underestimate the annual-mean northward meridional wind on the equator east of 150°W . Meridional wind errors are on the order of the observed wind and vary widely among models. To some degree the underestimate of the southerlies is due to cancellation of the meridional wind over the seasonal cycle associated with the alternating ITCZ error. The limited ability of models to simulate accurate wind stress on the ocean in such proximity to the Andes Mountains is not surprising. The Andes are narrow and tall, and poorly resolved by the horizontal and vertical coordinates used in large-scale models.

The spread of the SST among the models in the far-east equatorial region (2°N – 2°S , 80° – 90°W) is correlated to their meridional wind there at -0.66 (Fig. 11). The speed of model meridional wind varies from the observed value of 5 m s^{-1} to virtually zero, while SST varies from 24.2° to 27.2°C , except for model 2. Model SST is about 0.6°C cooler per m s^{-1} of meridional wind speed. Some models (notably models 7 and d) have the right mean scalar meridional wind speed for the wrong reason: they have strong unobserved northerlies in boreal spring. These spurious northerly winds nevertheless cool the equatorial SST. Even despite the interference of the annual cycle of winds, the correlation be-

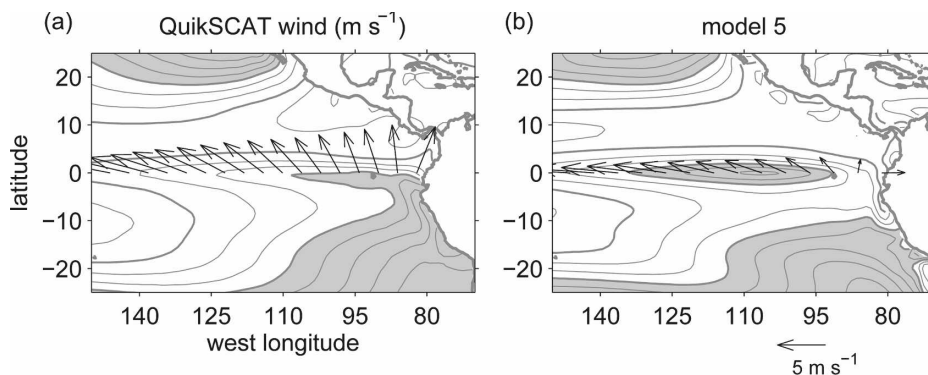


FIG. 10. Annual mean SST and equatorial wind (a) observed and (b) simulated by model 5 (Table 2). SST contour interval is 1°C ; SST below 24°C is shaded.

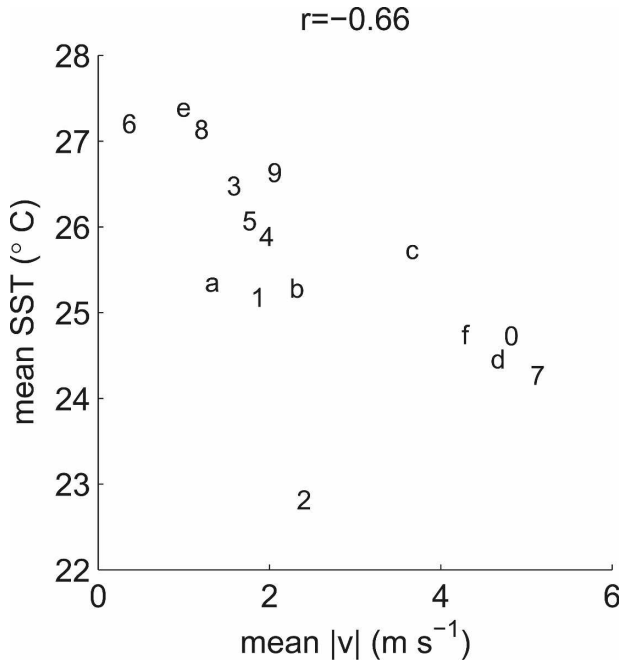


FIG. 11. Scatterplot of annual-average SST ($^{\circ}\text{C}$) and meridional wind speed (m s^{-1}) on the equator east of the Galápagos (2°N – 2°S , 80° – 90°W) for coupled models and observations. Plot symbols are as in Table 2.

tween the annual-mean meridional wind and the equatorial SST is -0.54 .

SST anomalies in the east due to wind errors near the shore may affect the development of the cold tongue to the west through a Bjerknes (1969) feedback, whereby winds diverge westward from the surface high pressure over the cold SST, further tilting the thermocline and lowering SST in the east (Xie 1998). SST and wind stress anomalies propagate westward, and in turn could affect the strength and location of convection in the western Pacific. Through Bjerknes feedback, a warm SST error near the coast and a cool SST error in the

central equatorial Pacific may partly compensate. A reversed zonal gradient of SST reverses the direction of the pressure gradient and wind, and changes the propagation of the Bjerknes feedback.

c. Central American isthmus winds

Strong northeasterly jets emerge onto the eastern Pacific warm pool from the Tehuantepec, Papagayo, and Panama gaps in the Central American Cordillera. These jets cool the ocean surface by enhancing evaporation and ocean vertical mixing, and induce upwelling in regions where they impose cyclonic wind stress curl (Kessler 2002; Xie et al. 2005; reviewed in Kessler 2006). For instance, a -0.5°C SST anomaly, associated with a thermocline dome known as the Costa Rica Dome, persists into summer and reduces the local precipitation over it. The jets depend on the interaction of the seasonal cycle of sea level pressure with the orographic effect of the narrow mountains of Central America, so their accurate representation is a challenging test of general circulation models (Xu et al. 2005). Some models resolve the three gap jets distinctly, while most models in the current study have a single broad jet corresponding to the poorly resolved orography of the Central American isthmus. Anomalies of the cross-isthmus gradient of SST and sea level pressure, such as could arise from model error or climate change, also affect the strength of the gap winds (Zhang and Delworth 2005).

The Tehuantepec, Papagayo, and Panama jets affect the SST of the northeast tropical Pacific warm pool. Figure 12a shows the December–February average wind vectors and SST from QuikSCAT and Reynolds et al. (2002) observations. The SST has anomalously positive and negative patches southwest of the Central American shore as a result of the curl of the wind jets, and the warm pool persists in the Northern Hemisphere

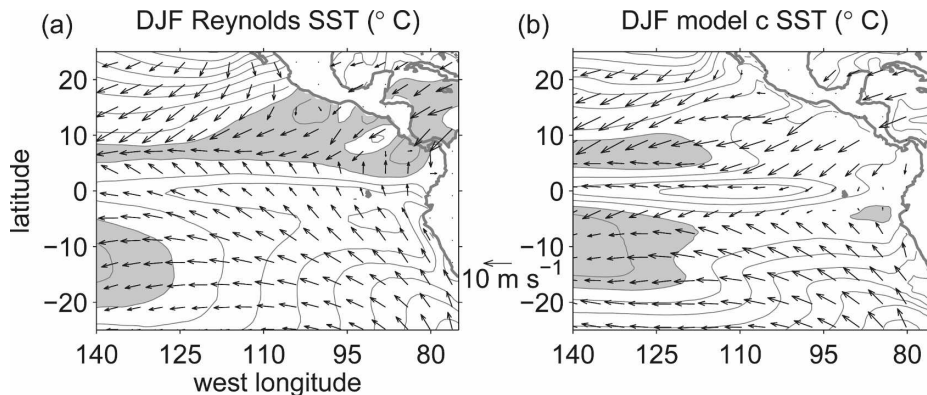


FIG. 12. December–February average wind vectors and SST ($^{\circ}\text{C}$) in (a) observations and (b) model c (Table 2). SST contour interval is 1°C ; SST contours above 27°C are shaded.

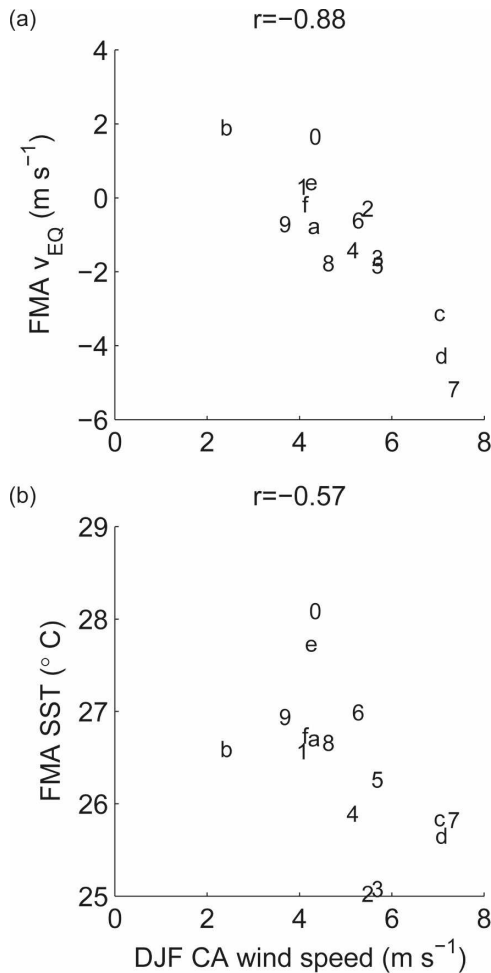


FIG. 13. Scatterplot of December–February (DJF) Central American Pacific (5° – 20° N, 80° – 110° W) wind speed vs February–April (FMA) (a) meridional wind within 2° of the equator and (b) SST in the Central American Pacific.

through boreal winter. SST in the Pacific southwest of Central America (5° – 20° N, 80° – 110° W) in February–April is slightly warmer than 28° C, yet in all the models it is cooler than 28° C (Fig. 13b). The correlation of February–April meridional wind on the equator to prior December–February northeasterlies in the Central American Pacific is -0.88 (Fig. 13a). Stronger wind speed in December–February is also correlated to cooler Central American Pacific SST in February–April in the models ($r = -0.57$; Fig. 13b). Strong winds presumably cool SST by evaporation and mixing and by Ekman pumping beneath cyclonic wind shear. Without being an extreme outlier, model c exhibits strong gap winds and cool SST in December–February (Fig. 12b). Compared to observations the northeasterlies are 2 – 5 m s^{-1} too strong, and the temperature east of 110° W is 2° C too cold in model c. While in observations the

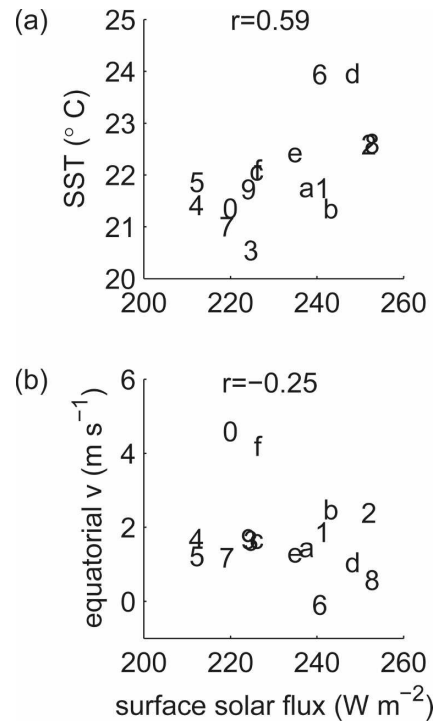


FIG. 14. Downward surface solar radiative flux vs (a) SST for observations and models in the southeastern stratus region (25° – 10° S, 80° – 95° W), and vs (b) equatorial meridional wind ($\pm 2^{\circ}$ lat).

northern ITCZ persists year round, excessive north-easterlies in model c are related to the end of the northern ITCZ and the migration of convection to the Southern Hemisphere in December.

d. Stratus clouds in the Southern Hemisphere

Deterministic model studies have shown that cooling the Southern Hemisphere ocean and marine atmospheric boundary layer by shading it with more stratus and stratocumulus clouds enhances the meridional asymmetry of the climate (Ma et al. 1996; Gordon et al. 2000b; Wang et al. 2004b, 2005; de Szoeke et al. 2006). The downward surface solar radiation of the observed climate is provided by the International Satellite Cloud Climatology Project (ISCCP) (Zhang et al. 2004; Rossow and Schiffer 1999) flux profile dataset. Assuming that solar forcing and clear-sky solar attenuation are essentially the same in all models, differences in the downwelling solar radiation among models are due to differences in the clouds. In the Southern Hemisphere stratus region (10° – 25° S, from the American coast to 95° W) intermodel variation in surface solar radiation (210 – 250 W m^{-2}) is significantly correlated to SST (20.5° – 24° C) at $r = 0.59$ (Fig. 14a), but not to the meridional wind on the equator ($r = -0.25$), an indicator of the meridional asymmetry of the climate.

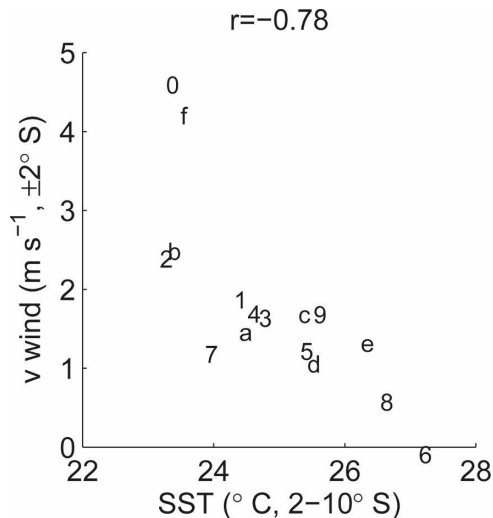


FIG. 15. Meridional wind on the equator (2°S – 2°N , 80° – 95°W) vs SST south of the equator (10° – 2°S , 80° – 95°W).

It is interesting to note that ISCCP surface solar radiation (220 W m^{-2}) is bounded by models on either side. In particular, the GFDL models have solar flux 8 W m^{-2} less than ISCCP, and the INM model has solar flux $\sim 1 \text{ W m}^{-2}$ less than ISCCP, indicating that clouds in these models have even stronger radiative forcing than estimated by ISCCP. The spatial pattern of solar radiation reaching the surface is complex and varies widely among the models (not shown). Most models have a clear region contouring the Peruvian and Chilean coast with solar flux greater than 250 W m^{-2} , while in ISCCP the coastal region is cloudy with solar radiation less than 200 W m^{-2} . This coastal cloud seems to be responsible for much of the systematic discrepancy between ISCCP and the models. In the region 80° – 95°W , cloud radiative cooling is stronger than in ISCCP for 3 of the 14 models. Nevertheless, in all models wind on the equator is weaker than QuikSCAT. Therefore the weakness and variation of meridional asymmetry among the models must be due to errors besides the simulation of stratiform clouds.

SST north of the main stratus region (2° – 10°S , 80° – 95°W) is correlated to the meridional wind on the equator at -0.78 (Fig. 15), but not to the local solar radiation there. North of 10°S stratiform clouds share the sky with convective clouds. Both cloud types shade the surface from solar radiation. While convective clouds are associated with heating and surface convergence, stratiform clouds are associated with cooling and divergence. As a result of the canceling dynamic effect of stratiform and convective clouds, correlations between the wind and solar radiation are insignificantly small. The lack of intermodel correlation between asymmetry of the cir-

ulation and solar radiation does not disprove the relationship between the cooling effect of stratus clouds and the atmospheric meridional circulation. Rather, the intermodel correlation may not be an effective test of this relationship. Furthermore, though surface solar radiation is a key diagnostic of the surface heat budget, it cannot dissect the complex and parameterized interaction between cumulus and stratus clouds.

4. Summary

Simulation of the seasonal cycle of the tropical eastern Pacific by general circulation models has improved in the years since the study of Mechoso et al. (1995). The weak seasonal cycle and lack of asymmetry of SST and precipitation about the equator associated with a persistent double ITCZ error in most models of 1995 is improved in most models today, even in models without flux adjustment. The persistent double ITCZ has largely given way to a strong seasonal cycle and an alternating ITCZ error in which the warm pool of SST and the ITCZ rainband alternate hemispheres following the meridional migration of solar heating. Eight of the 15 models assessed in this study exhibited an alternating ITCZ error. Many models also have a cold SST error on the equator and extension of the equatorial cold tongue too far to the west. In many models the equatorial ocean is too warm between the Galápagos and the west coast of South America.

In the zonal average, models are clearly differentiated by their simulation of the latitude of warm SST and rain associated with the ITCZ throughout the seasonal cycle (Fig. 5). The various seasonal–meridional distributions of heating in the simulations give rise to different cycles of wind on the equator, which in turn affect the seasonal cycle of the equatorial cold tongue temperature. Error in the seasonal–meridional cycle of the simulations is largely explained by the mean meridional asymmetry of SST and rain and the amplitude of the seasonal cycle of the asymmetry.

The ensemble of simulations in this study suggests that the erroneous demise of the northern ITCZ and its shift into the Southern Hemisphere in boreal spring generates a northerly wind speed maximum on the equator. Meridional wind in either direction drives a meridional–vertical overturning on the equator with upwelling on the windward side of the equator causing a net cooling of the equator. Spurious northerlies in spring thus cool the equator, so models with an alternating ITCZ have a semiannual cycle of upwelling and mixing on the equator, a cold SST error in March, and a net cold SST error on the equator. March SST varies from 22° to 27°C among models, whereas it is 27°C in observations.

For some models with high resolution of the equatorial ocean, inclusion of the Galápagos Archipelago has been shown to alleviate SST errors in the eastern equatorial Pacific (Eden and Timmermann 2004; Karnauskas et al. 2007). Experiments adding and removing the Galápagos from IROAM showed little difference in the far-field SST and currents. None of the ocean models analyzed here have grid-averaged bathymetry reaching the surface. Two models with high resolution, IROAM ($0.5^\circ \times 0.5^\circ$) and MIROC3.2(hires) (1° latitude \times 2° longitude), have Galápagos seamounts within 300 m of the surface and equatorial SST close to observations (24.9°C over 140° – 90°W), among the warmer third of models.

Many of the current generation of GCMs have a primary or secondary peak in interannual variability in boreal summer, approximately six months out of phase from the observed peak in December (Saji et al. 2006). Is there a physical mechanism linking upwelling under spurious spring northerlies and the season of peak interannual variability? Work is underway to diagnose the seasonal cycle of equatorial coupled atmosphere–ocean Bjerknes instability (Jin et al. 2006; K. J. Stein 2007, personal communication). Zonal wind stress on the equator is observed to be weak in March–May when the cross-equatorial wind is also minimal. The effect of the cross-equatorial wind on the zonal wind should be investigated, as the seasonal cycle of zonal wind in the Niño-4 region (160°E – 150°W) affects ENSO and is not well simulated by many models (Guillard 2006).

The simulation of meridional wind on the equator contributes to the warm equatorial SST error east of the Galápagos. Easterly trade winds are observed to weaken toward the shore. In their absence southerly meridional wind is critical for generating upwelling south of the equator. Simulations with strong meridional wind speed on the equator between 80° – 90°W have colder SST there, while models with weak meridional wind develop a warm error. The meridional wind here is likely influenced by model representation of the steep and narrow Andes mountain range, which varies with the resolution and numerical schemes employed in the various models. The equatorial southerlies between the Galápagos and South America are correlated at 0.63 to the peak height of the Andes Cordillera (north of 15°S) in the models. Continental and orographic effects on the atmosphere could contribute to the variety of model simulations of wind offshore of South America. Relationships between wind and coastal ocean upwelling, and amplification of the asymmetry by wind–evaporation–SST (WES) feedback (Xie 2004; Lin 2007) also vary among models.

The influence of mountains on wind over the ocean is underscored by the winds passing through gaps in the Central American Cordillera. In boreal winter, the North Atlantic subtropical high drives Caribbean low-level jet northeasterlies, which blow through passes in the cordillera onto the northeast tropical Pacific (Amador 1998; Wang and Lee 2007). If these winds blow too strongly on the eastern Pacific warm pool, as in some models, then SST can cool so much as to contribute to the early demise of the northern ITCZ and the establishment of a dominant southern ITCZ. The correlation of February–April SST in the Central American eastern Pacific to the wind speed two months prior is -0.57 . The even stronger correlation among simulations ($r = -0.88$) of equatorial meridional wind following the Central American northeasterlies suggests that an atmospheric or ocean–atmosphere feedback could reinforce the shift of the ITCZ into the Southern Hemisphere.

Cooling by stratus clouds is but one of many factors influencing the meridional circulation of the atmosphere in the eastern Pacific. Representation of the cloud radiative effect is not the dominant source of error among the models analyzed, yet representation of stratus clouds might significantly influence the meridional atmospheric circulation, especially in the absence of other model errors.

According to the heat flux required of the ocean (advection, upwelling, and mixing) to balance the net surface heat flux and maintain the annual-average SST, the ocean cools the surface by more than -100 W m^{-2} along the equator and South American coast. The strength of equatorial cooling and strength and distribution of coastal cooling differ considerably among models (not shown). Some models (IAP, INM, IPSL, NCAR CCSM3, and PCM1) simulate noticeably more cooling by the ocean north of the equator than south, contributing to their lack of meridional asymmetry. We suspect this error is another symptom of a too-strong northerly wind driving offshore Ekman transport and upwelling along the coast in the Northern Hemisphere.

Acknowledgments. This work has been funded by the Japanese Ministry of Education, Culture, Sports, Science and Technology (MEXT) as category 7 of the RR2002 Project, by JAMSTEC, by NOAA, and by the National Research Council. The authors are grateful to N. H. Saji for downloading and computing climatologies of most of the 20C3M simulations, Jan Hafner for computing the QuikSCAT climatology, and R. Justin Small for helpful discussion. The authors also wish to thank W. S. Kessler and the anonymous reviewer for their insightful comments on the manuscript. Quik-

SCAT data are produced by Remote Sensing Systems and sponsored by the NASA Ocean Vector Winds Science Team. The TRMM 3B43 observations were provided by the Asia Pacific Data Research Center (APDRC; additional information is available online at <http://apdrc.soest.hawaii.edu/>). The numerical calculation of IROAM was carried out at the Earth Simulator Center. APDRC was instrumental in providing access to the IROAM data.

REFERENCES

- AchutaRao, K., and K. R. Sperber, 2006: ENSO simulation in coupled ocean-atmosphere models: Are the current models better? *Climate Dyn.*, **27**, 1–15.
- Adler, R. F., G. J. Huffman, D. T. Bolvin, S. Curtis, and E. J. Nelkin, 2000: Tropical rainfall distributions determined using TRMM combined with other satellite and rain gauge information. *J. Appl. Meteor.*, **39**, 2007–2023.
- Amador, J. A., 1998: A climatic feature of the tropical Americas: The trade wind easterly jet. *Trop. Meteor. Oceanogr.*, **5**, 91–102.
- Bjerknes, J., 1969: Atmospheric teleconnections from the equatorial Pacific. *Mon. Wea. Rev.*, **97**, 163–172.
- Cai, W. J., H. H. Hendon, and G. Meyers, 2005: Indian Ocean dipolelike variability in the CSIRO mark 3 coupled climate model. *J. Climate*, **18**, 1449–1468.
- Carton, J. A., G. Chepurin, X. H. Cao, and B. Giese, 2000a: A simple ocean data assimilation analysis of the global upper ocean 1950–95. Part I: Methodology. *J. Phys. Oceanogr.*, **30**, 294–309.
- , —, and —, 2000b: A simple ocean data assimilation analysis of the global upper ocean 1950–95. Part II: Results. *J. Phys. Oceanogr.*, **30**, 311–326.
- Collins, W. D., and Coauthors, 2006: The Community Climate System Model version 3 (CCSM3). *J. Climate*, **19**, 2122–2143.
- Dai, A. G., 2006: Precipitation characteristics in eighteen coupled climate models. *J. Climate*, **19**, 4605–4630.
- Davey, M. K., and Coauthors, 2002: STOIC: A study of coupled model climatology and variability in tropical ocean regions. *Climate Dyn.*, **18**, 403–420.
- Delworth, T. L., and Coauthors, 2006: GFDL's CM2 global coupled climate models. Part I: Formulation and simulation characteristics. *J. Climate*, **19**, 643–674.
- de Szoeke, S. P., and C. S. Bretherton, 2004: Quasi-Lagrangian large eddy simulations of cross-equatorial flow in the east Pacific atmospheric boundary layer. *J. Atmos. Sci.*, **61**, 1837–1858.
- , Y. Wang, S.-P. Xie, and T. Miyama, 2006: Effect of shallow cumulus convection on the eastern Pacific climate in a coupled model. *Geophys. Res. Lett.*, **33**, L17713, doi:10.1029/2006GL026715.
- Diansky, N. A., and E. M. Volodin, 2002: Simulation of present-day climate with a coupled atmosphere-ocean general circulation model. *Izv. Atmos. Oceanic Phys.*, **38**, 732–747.
- Eden, C., and A. Timmermann, 2004: The influence of the Galápagos Islands on tropical temperatures, currents and the generation of tropical instability waves. *Geophys. Res. Lett.*, **31**, L15308, doi:10.1029/2004GL020060.
- Flato, G. M., and G. J. Boer, 2001: Warming asymmetry in climate change simulations. *Geophys. Res. Lett.*, **28**, 195–198.
- Goosse, H., and T. Fichefet, 1999: Importance of ice-ocean interactions for the global ocean circulation: A model study. *J. Geophys. Res.*, **104**, 337–355.
- Gordon, C., C. Cooper, C. A. Senior, H. Banks, J. M. Gregory, T. C. Johns, J. F. B. Mitchell, and R. A. Wood, 2000a: The simulation of SST, sea ice extents and ocean heat transports in a version of the Hadley Centre coupled model without flux adjustments. *Climate Dyn.*, **16**, 147–168.
- Gordon, C. T., A. Rosati, and R. Gudgel, 2000b: Tropical sensitivity of a coupled model to specified ISCCP low clouds. *J. Climate*, **13**, 2239–2260.
- Guilyardi, E., 2006: El Niño mean state-seasonal cycle interactions in a multi-model ensemble. *Climate Dyn.*, **26**, 329–348.
- Horel, J. D., and J. M. Wallace, 1981: Planetary-scale atmospheric phenomena associated with the Southern Oscillation. *Mon. Wea. Rev.*, **109**, 813–829.
- Jin, F.-F., S. T. Kim, and L. Bejarano, 2006: A coupled-stability index for ENSO. *Geophys. Res. Lett.*, **33**, L23708, doi:10.1029/2006GL027221.
- Karnauskas, K. B., R. Murtugudde, and A. J. Busalacchi, 2007: The effect of the Galápagos Islands on the equatorial Pacific cold tongue. *J. Phys. Oceanogr.*, **37**, 1266–1281.
- Kessler, W. S., 2002: Mean three-dimensional circulation in the northeast tropical Pacific. *J. Phys. Oceanogr.*, **32**, 2457–2471.
- , 2006: The circulation of the eastern tropical Pacific: A review. *Prog. Oceanogr.*, **69**, 181–217.
- , L. M. Rothstein, and D. K. Chen, 1998: The annual cycle of SST in the eastern tropical Pacific, diagnosed in an ocean GCM. *J. Climate*, **11**, 777–799.
- Kistler, R., and Coauthors, 2001: The NCEP–NCAR 50-Year Reanalysis: Monthly means CD-ROM and documentation. *Bull. Amer. Meteor. Soc.*, **82**, 247–267.
- Large, W. G., and G. Danabasoglu, 2006: Attribution and impacts of upper-ocean biases in CCSM3. *J. Climate*, **19**, 2325–2346.
- Levitus, S., and A. H. Oort, 1977: Global analysis of oceanographic data. *Bull. Amer. Meteor. Soc.*, **58**, 1270–1284.
- Lin, J.-L., 2007: The double-ITCZ problem in IPCC AR4 coupled GCMs: Ocean–atmosphere feedback analysis. *J. Climate*, **20**, 4497–4525.
- Ma, C.-C., C. R. Mechoso, A. W. Robertson, and A. Arakawa, 1996: Peruvian stratus clouds and the tropical Pacific circulation: A coupled ocean–atmosphere GCM study. *J. Climate*, **9**, 1635–1645.
- Mechoso, C. R., and Coauthors, 1995: The seasonal cycle over the tropical Pacific in coupled ocean–atmosphere general circulation models. *Mon. Wea. Rev.*, **123**, 2825–2838.
- Meehl, G. A., P. R. Gent, J. M. Arblaster, B. L. Otto-Bliesner, E. C. Brady, and A. Craig, 2001: Factors that affect the amplitude of El Niño in global coupled climate models. *Climate Dyn.*, **17**, 515–526.
- , W. M. Washington, W. D. Collins, J. M. Arblaster, A. Hu, L. E. Buja, W. G. Strand, and H. Teng, 2005: How much more global warming and sea level rise? *Science*, **307**, 1769–1772.
- Mitchell, T. P., and J. M. Wallace, 1992: The annual cycle in equatorial convection and sea surface temperature. *J. Climate*, **5**, 1140–1156.
- Neelin, J. D., D. S. Battisti, A. C. Hirst, F.-F. Jin, Y. Wakata, T. Yamagata, and S. E. Zebiak, 1998: ENSO theory. *J. Geophys. Res.*, **103**, 14 261–14 290.
- Nozawa, T., T. Nagashima, H. Shiogama, and S. A. Crooks, 2005: Detecting natural influence on surface air temperature change in the early twentieth century. *Geophys. Res. Lett.*, **32**, L20719, doi:10.1029/2005GL023540.

- Okajima, H., S. P. Xie, and A. Numaguti, 2003: Interhemispheric coherence of tropical climate variability: Effect of the climatological ITCZ. *J. Meteor. Soc. Japan*, **81**, 1371–1386.
- Pacanowski, R. C., 1995: MOM 2 documentation, user's guide, and reference manual, Version 1.0. GFDL Ocean Group Tech. Rep. 3, 232 pp.
- , and S. M. Griffies, cited 2000: MOM 3.0 manual. NOAA/Geophysical Fluid Dynamics Laboratory. [Available online at http://www.gfdl.noaa.gov/~smg/MOM/web/guide_parent/guide_parent.html.]
- Philander, S. G. H., and R. C. Pacanowski, 1981: The oceanic response to cross-equatorial winds (with application to coastal upwelling in low latitudes). *Tellus*, **33**, 201.
- , and P. Delecluse, 1983: Coastal currents in low latitudes (with application to the Somali and El Niño currents). *Deep-Sea Res.*, **30A**, 887–902.
- , D. Gu, D. Halpern, G. Lambert, N. C. Lau, T. Li, and R. C. Pacanowski, 1996: Why the ITCZ is mostly north of the equator. *J. Climate*, **9**, 2958–2972.
- Polito, P. S., J. P. Ryan, W. T. Liu, and F. P. Chavez, 2001: Oceanic and atmospheric anomalies of tropical instability waves. *Geophys. Res. Lett.*, **28**, 2233–2236.
- Reynolds, R. W., N. A. Rayner, T. M. Smith, D. C. Stokes, and W. Wang, 2002: An improved in situ and satellite SST analysis for climate. *J. Climate*, **15**, 1609–1625.
- Richter, I., and C. R. Mechoso, 2006: Orographic influences on subtropical stratocumulus. *J. Atmos. Sci.*, **63**, 2585–2601.
- Rossow, W. B., and R. A. Schiffer, 1999: Advances in understanding clouds from ISCCP. *Bull. Amer. Meteor. Soc.*, **80**, 2261–2287.
- Saji, N. H., S.-P. Xie, and T. Yamagata, 2006: Tropical Indian Ocean variability in the IPCC twentieth-century climate simulations. *J. Climate*, **19**, 4397–4417.
- Salas-Méllia, D., and Coauthors, 2005: Description and validation of the CNRM-CM3 global coupled model. CNRM Tech. Rep. 103, 36 pp. [Available online at http://www.cnrm.meteo.fr/scenario2004/paper_CM3.pdf.]
- Small, R. J., S.-P. Xie, Y. Wang, S. K. Esbensen, and D. Vickers, 2005: Numerical simulation of boundary layer structure and cross-equatorial flow in the eastern Pacific. *J. Atmos. Sci.*, **62**, 1812–1830.
- Taylor, K. E., 2001: Summarizing multiple aspects of model performance in a single diagram. *J. Geophys. Res.*, **106D**, 7183–7192.
- Wallace, J. M., and D. S. Gutzler, 1981: Teleconnections in the geopotential height field during the Northern Hemisphere winter. *Mon. Wea. Rev.*, **109**, 784–812.
- , E. M. Rasmusson, T. P. Mitchell, V. E. Kousky, E. S. Sarachik, and H. von Storch, 1998: The structure and evolution of ENSO-related climate variability in the tropical Pacific: Lessons from TOGA. *J. Geophys. Res.*, **103C**, 14 241–14 259.
- Wang, C., and S.-K. Lee, 2007: Atlantic warm pool, Caribbean low-level jet, and their potential impact on Atlantic hurricanes. *Geophys. Res. Lett.*, **34**, L02703, doi:10.1029/2006GL028579.
- Wang, Y., O. L. Sen, and B. Wang, 2003: A highly resolved regional climate model (IPRC-RegCM) and its simulation of the 1998 severe precipitation event over China. Part I: Model description and verification of simulation. *J. Climate*, **16**, 1721–1738.
- , S.-P. Xie, H. Xu, and B. Wang, 2004a: Regional model simulations of marine boundary layer clouds over the southeast Pacific off South America. Part I: Control experiment. *Mon. Wea. Rev.*, **132**, 274–296.
- , H. Xu, and S.-P. Xie, 2004b: Regional model simulations of marine boundary layer clouds over the southeast Pacific off South America. Part II: Sensitivity experiments. *Mon. Wea. Rev.*, **132**, 2650–2668.
- , S.-P. Xie, B. Wang, and H. Xu, 2005: Large-scale atmospheric forcing by southeast Pacific boundary layer clouds: A regional model study. *J. Climate*, **18**, 934–951.
- Wittenberg, A. T., A. Rosati, N. C. Lau, and J. J. Ploshay, 2006: GFDL's CM2 global coupled climate models. Part III: Tropical Pacific climate and ENSO. *J. Climate*, **19**, 698–722.
- Xie, S.-P., 1994: On the genesis of the equatorial annual cycle. *J. Climate*, **7**, 2008–2013.
- , 1998: Ocean–atmosphere interaction in the making of the Walker circulation and equatorial cold tongue. *J. Climate*, **11**, 189–201.
- , 2004: The shape of continents, air–sea interaction, and the rising branch of the Hadley circulation. *The Hadley Circulation: Past, Present and Future*, H. F. Diaz and R. S. Bradley, Eds., Kluwer Academic Publishers, 121–152.
- , and K. Saito, 2001: Formation and variability of a northerly ITCZ in a hybrid coupled AGCM: Continental forcing and oceanic–atmospheric feedback. *J. Climate*, **14**, 1262–1276.
- , H. M. Xu, W. S. Kessler, and M. Nonaka, 2005: Air–sea interaction over the eastern Pacific warm pool: Gap winds, thermocline dome, and atmospheric convection. *J. Climate*, **18**, 5–20.
- , and Coauthors, 2007: A regional ocean–atmosphere model for eastern Pacific climate: Toward reducing tropical biases. *J. Climate*, **20**, 1504–1522.
- Xu, H., Y. Wang, and S.-P. Xie, 2004: Effects of the Andes on eastern Pacific climate: A regional atmospheric model study. *J. Climate*, **17**, 589–602.
- , S.-P. Xie, Y. Wang, and R. J. Small, 2005: Effects of Central American mountains on the eastern Pacific winter ITCZ and moisture transport. *J. Climate*, **18**, 3856–3873.
- Yu, Y. Q., X. H. Zhang, and Y. F. Guo, 2004: Global coupled ocean–atmosphere general circulation models in LASG/IAP. *Adv. Atmos. Sci.*, **21**, 444–455.
- Yukimoto, S., and Coauthors, 2001: The new Meteorological Research Institute coupled GCM (MRI-CGCM2). Model climate and variability. *Pap. Meteor. Geophys.*, **51**, 47–88.
- Zhang, R., and T. L. Delworth, 2005: Simulated tropical response to a substantial weakening of the Atlantic thermohaline circulation. *J. Climate*, **18**, 1853–1860.
- Zhang, Y. C., W. B. Rossow, A. A. Lacis, V. Oinas, and M. I. Mishchenko, 2004: Calculation of radiative fluxes from the surface to top of atmosphere based on ISCCP and other global data sets: Refinements of the radiative transfer model and the input data. *J. Geophys. Res.*, **109**, D19105, doi:10.1029/2003JD004457.